MD 3584: Long-Range Beam-Beam 2018

N. Karastathis, S. Fartoukh, S. Kostoglou, Y. Papaphilippou, M. Pojer,
A. Poyet, M. Solfaroli, G. Sterbini
CERN, CH-1217 Meyrin, Switzerland

Summary

A recurrent issue of the LHC operation, observed both during Run1 and Run2 is the asymmetric behaviour of the two beams in terms of particle losses. The fact that Beam 1 shows higher losses when compared to Beam 2 is not intuitive, especially when compared to the symmetric design of the two rings. The beam-beam effects induced by the interaction of the two beams in the experimental inserts, as well as noise sources contribute to the degradation of the beam lifetime, possibly asymmetrically between the two beams. In this Machine Development study, several machine and beam configurations are considered to identify or discard some of the possible sources of this behaviour. The impact of the active filters of the main bends in the beam spectrum is tested at injection energy as a possible source of $50\,\mathrm{Hz}$ harmonics. A variation in the beam-beam separation induced by a crossing angle bias, and the impact of the optics choice of different phase advances between the two high-luminosity interaction points are scrutinized as source of lifetime asymmetry. Finally, the wire beam-beam compensator is tested for the first time with full beam in a sub-optimal configuration and its impact is assessed.

Contents

1 Motivation

The design of the Large Hadron Collider (LHC) is symmetric between the two rings in which the counter-rotating beams are circulating. However, observations during Run1 and Run2 have revealed a significant asymmetry in the lifetime of the two beams, especially during collisions where the lifetime is dominated by the interactions at the 4 main interaction points (IP) in the insertion regions (IR) which house the main experiments. These beam-beam interactions have been studied in the past systematically, both in the head-on (HO) regime, when two bunches overlap, as well as when the Coulomb forces act from distance, i.e., in the long-range (LR) beam-beam regime [1, 2, 3, 4, 5, 6, 7]. However, so far there are no conclusive results concerning the lifetime imbalance.

New observations from the proton production fills suggest that the diffusive mechanisms such as beam-beam and/or the electron cloud effects create a significant imbalance of the two beams. Figure 1 shows the evolution of the lifetime imbalance of the two beams within a fill. The statistics include all the proton production fills and separate the different beam flavours (BCMS and 8b+4e) that have been used in the 2017 run. The fills with the 8b+4e beams which by construction have less LR interactions and less electron cloud effect show less lifetime imbalance compared to the BCMS ones.
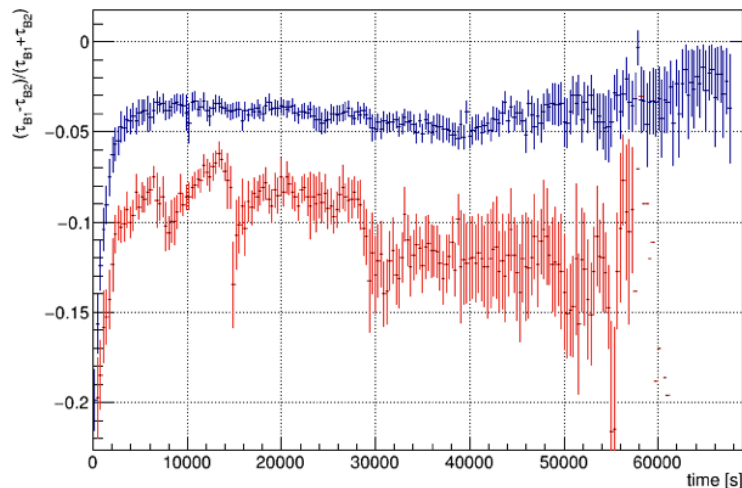

Figure 1: The lifetime imbalance between Beam 1 and Beam 2 for the 2017 run as a function of the time in the fill. The red curve corresponds to the average of the fills using a BCMS injected beam, while the blue to the 8b4e bunch scheme.

Focusing on the beam-beam interactions, as electron cloud studies have been performed in parallel [8], a campaign to identify possible effects that induce a bias in the lifetime of one of the two beams have been launched. One speculation is that in one of the two high-luminosity IPs (IP1 and IP5), where the beam-beam force is stronger, there is a systematic offset in the crossing angle of one of the two beams. The effect of such an offset would be to change the design beam-beam separation in one of the two sides of an IP, while maintaining the same crossing angle at the IP. Furthermore, an additional candidate could be the effect of the optics design in the form of the phase advance between the two IPs. In fact, by design, the phase advance between IP1 and IP5 are different between the two beams: a difference

of $38°$ in $\Delta\mu_x$ for for Beam 2 (B2) compared to Beam 1 (B1), as well as a $41°$ in $\Delta\mu_y$. Changing this phase advance for one of the two beams have shown a non-negligible effect in the lifetime of the beams both in colliding [9], such as in Fig. 2, and non-colliding [10] beams. In this MD, the B1 lifetime is tested as function of phase advance between IP1 and IP5 trying to reproduce the results of MD3263 (Fig. 2).
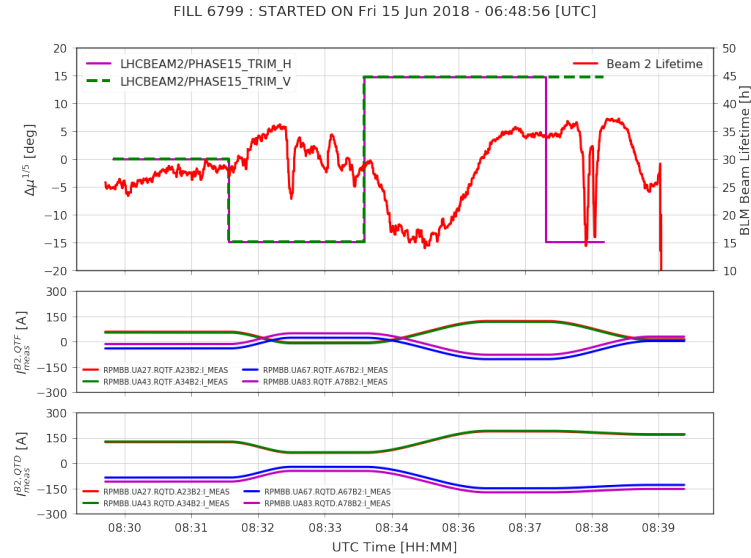

Figure 2: The impact of the trims in the phase advance between IP1 and IP5 of B2 on its lifetime. A slight trend is observed during MD3263 in 2018 (FILL 6799).

The last test in the MD during collisions is to assess the impact of the DC wires on the beam lifetime. A campaign has been launched since 2017, when the wires have been installed in IR1 and IR5 for B2, to prove their beneficial impact on the beam lifetime by compensating the LR part of the beam-beam interactions [11]. A clear signature of compensation has been identified in the single bunch regime, when the wires are placed at a close distance from the beam. Here, the compensation is tested with the wire collimators being at their operationally nominal position (sub-optimal for the wire compensation) and, in addition, the effect is assessed for the first time with trains in B2.

Finally, another significant contribution for the beam lifetime and its B1-B2 unbalance could be related to the noise sources. A recurrent observation on the LHC transverse beam spectra is the existence of 50 Hz harmonics. Several studies have been taken place in the past [12, 13]. In this MD, a fill at injection energy is dedicated to study the effect of the Silicon Controlled Rectifiers converters on the main bending dipoles. The aim is to identify, by deactivating the active filters of these power supplies, if the observed frequency signals are a feature of the instrumentation or if the transverse motion of the beam is excited.

2   Preparation for the MD

Detailed studies have been performed, before the MD, to identify the optimal beam and machine conditions, as well as the proper observables in order to assist with the tests in the

machine. The tolerances of the available equipment have been studied in order to minimize the possibility to lose beam time due to beam dumps.

2.1 Crossing Angle Bias

For the crossing angle bias, two new knobs have been developed and registered in LSA. The knobs `IP1-XING-BIAS-V-MURAD` and `IP5-XING-BIAS-H-MURAD` induce a systematic bias in IP1 and IP5 respectively. When positive, the bias increases the crossing angle of B1 and reduces the one of B2, while keeping the crossing angle between the two beams constant. The value of the half-crossing angle between the two beams have been chosen at 130 µrad, while the maximum bias was set to ±30 µrad to keep the minimum crossing angle of any beam at the already commissioned value of 100 µrad. The effect of the crossing angle bias is to modify the extrema of the beam-beam separation around the IP. For example, the beam-beam separation in IR1 for the two beams is shown in Fig. 3, when for one beam the separation reduces, for the other beam it increases, therefore resulting in weaker beam-beam forces. It is worth noting that, in the simulations and during the measurement, the octupoles were powered at +550 A.
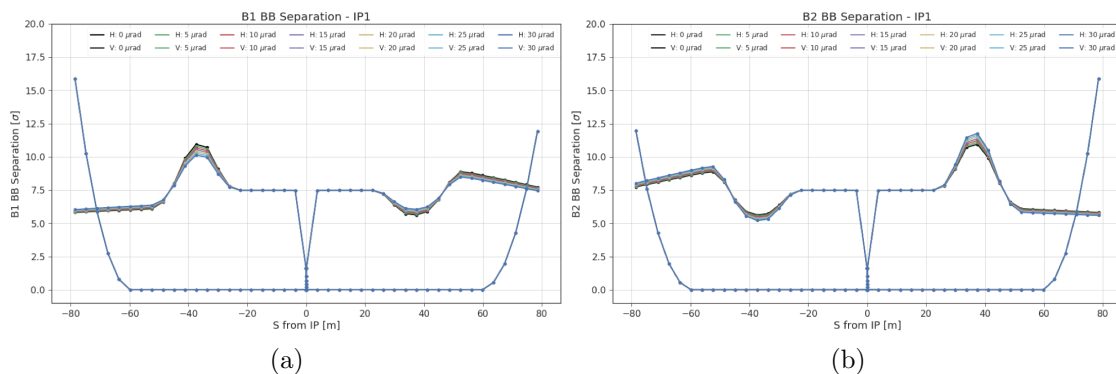

(a)   (b)

Figure 3: The effect of the crossing angle bias applied in IR1 on the beam-beam separation for B1 (a) and B2 (b). In each of the plots two sets of curves represent the horizontal and vertical beam-beam separation. Since, in IP1, the crossing is vertical, the crossing angle bias will affect only the vertical plane. The horizontal separation will be constant during the scan of the crossing angle bias knob and will be determined by the D1 separation dipole.

By changing the crossing angle bias, due to the dipolar feed-down of the triplet, the beam-beam long-range (BBLR) occurring in the triplets are modified and, with those, their BBLR quadrupolar effect. To identify if a tune feedback system has to be developed for this scan, the deviation from the initial working point is studied as a function of the crossing angle bias applied and the bunch intensity at which is applied. Figure 4 shows the result for this study in IR1. The overall change in the tune is at the level of 10^{-4}, thus no additional steps to control the tune have been considered.

In terms of operational implementation, the crossing angle bias is introduced by trimming the current of the MCB correctors around the IPs, the same correctors defining the crossing bumps. A set of software limits is defined on the current powering these magnets, which, if
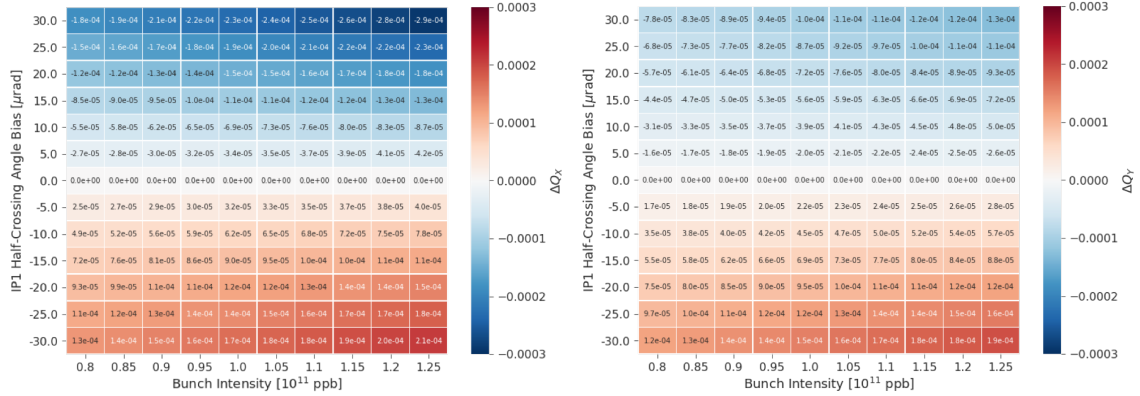
Figure 4: The impact of the crossing angle bias on the variation of the horizontal (a) and vertical (b) tune from the initial point as a function of the bunch intensity at which the bias is introduced. The deviation is considered negligible.

exceeded, will trigger a beam dump sequence in order to protect the machine from possible damage. A study on the tolerances of the correctors for the maximum planned crossing angle bias of ± 30 µrad is shown in Fig. 5a. All correctors can accommodate the required variation in current within their preset tolerances. Since these correctors are also used to define the crossing angle at the IP, and not only the bias, to increase the safety margin, the tolerances of the correctors have been slightly increased by the Engineer in Charge with a pre-defined sequence executed during the beam process.

A similar study has been performed for the orbit offset generated by the bias at the tertiary collimators around the IP1/5 that protect the triplet magnets. A small orbit offset at the position of the collimators is expected since the crossing angle bump is closed at ± 250 m around the IP. The orbit at a crossing angle of 130 µrad was compared to the ones of the 100 µrad and 160 µrad to identify the maximum crossing bias that could be applied at the starting point of 130 µrad, while the orbit still remains within the commissioned envelope of 100-160 µrad. The restricting points in both IPs are the tertiary collimators at the crossing plane of each IP, i.e., TCTPV in IR1 and TCTPH in IR5. Requesting no additional offset while including an orbit bump is de facto a strict requirement. With this requirement in place a maximum bias of ± 17 µrad can be applied in IR1 and ± 12 µrad in IR5. Figure 5b shows the offset in collimation beam sizes when applying the maximum crossing angle bias. A maximum of less than $0.5\,\sigma_{\mathrm{coll}}$[1] is found, which is compatible to the orbit offsets during a luminosity optimization scan. Therefore, without changing the collimator half-gaps, the full range of the bias can be accommodated around the IRs without producing any additional losses that could result in a beam dump.

Finally, beam-beam tracking simulations have been performed to identify the impact of the crossing angle bias on the Dynamic Aperture (DA) of the LHC. Figure 6 shows the results for IP1 and IP5. The results show no significant impact of the crossing angle bias. However these simulations include only the beam-beam interactions. Additional diffusive mechanisms, such as the effect of electron cloud are not simulated and could have a non-negligible impact on the results.

---

[1] The σ_{coll} represents the beam σ assuming a normalized emittance of 3.5 mm mrad.
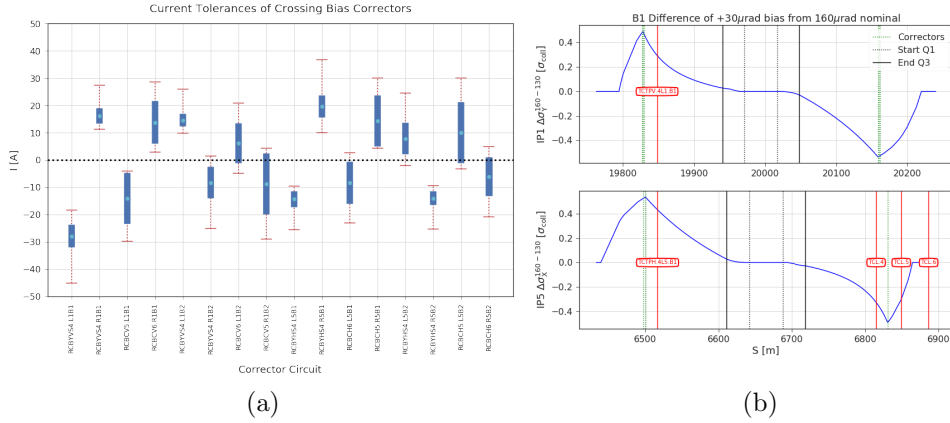
Figure 5: Studies for the corrector and collimator tolerances of the crossing angle bias knob. (a) The range, in terms of current tolerance, for all the correctors under use for the crossing angle bias scan. The red bars show the maximum tolerance in current of each corrector. The blue range shows the variation in current from inducing a bias of $\pm 30\,\mu$rad. (b) The orbit offset, in collimation beam sizes, at the two IRs if the maximum crossing bias is applied.
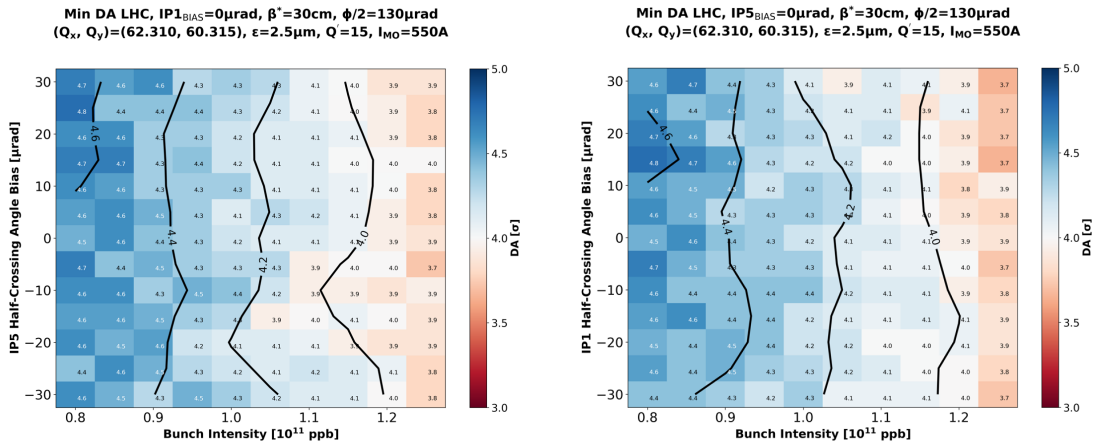

Figure 6: Dynamic aperture scans for the crossing angle bias as a function of the bunch intensity for IP1 and IP5. The simulation assumes a constant octupole current at 550 A (as in the experimental condition).

2.2 Phase Advance between IP1/5

Concerning the phase advance scan, two knobs have been implemented to change the phase advance between IP1 and IP5 for beam 1 for the horizontal and vertical plane, `LHCBEAM1/PHASE15_TRIM_H` and `LHCBEAM1/PHASE15_TRIM_V` respectively. The knob acts on the trim quadrupoles that are used for the tune control. Figure 7 shows the impact of the knobs in the tune setting of the machine. The impact of the knob on the working point of the machine is almost negligible for a variation of $\pm 9\,°$ on both planes, but a measurable impact can be found for larger dephasing values.
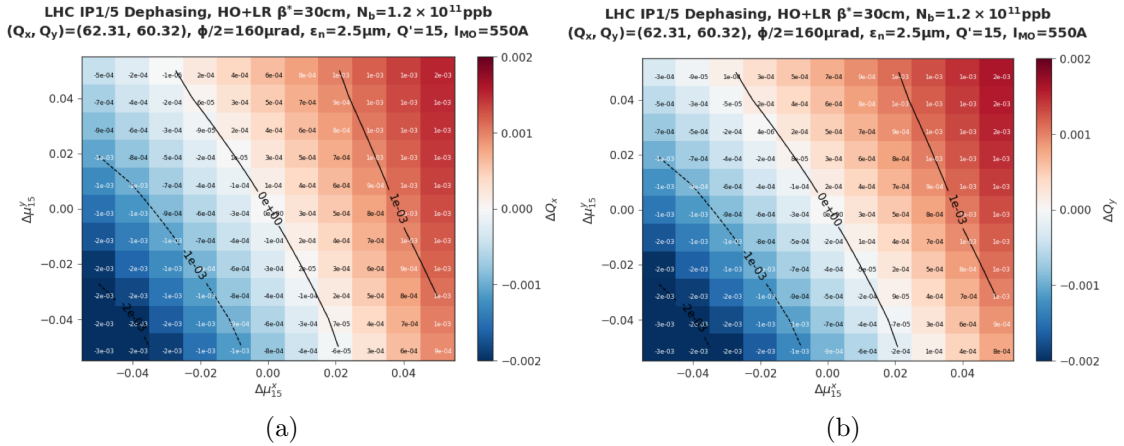
7

Figure 7: The effect of the dephasing of B1 between IP1 and IP5 on the horizontal (a) and vertical (b) detuning.

In order to symmetrize the phase advance of the two beams a dephasing of $38\,^\circ$ has to be applied in the horizontal plane and $41\,^\circ$ in the vertical. However, for machine protection concerns, the phase advance between the extraction kicker (MKD) and the tertiary collimators in the two IPs (TCT) has to be within a range of $150\,^\circ$-$210\,^\circ$. As shown in Figure 8a, the MKD-TCT in IR5 are always in phase, therefore the limiting IR is IR1. In IR1, no limit is found in the phase advance of the vertical plane, therefore the maximum of $40\,^\circ$ can be applied. However, on the horizontal plane a limit of $25\,^\circ$ is considered due to the phase advance between MKD.A and TCTPH.4L1.

Furthermore, aperture studies identified the MQXB.B2R5 as a limitation in the aperture of the machine, but no significant impact of the dephasing knob was found on the aperture of the machine. On the other hand, a modest β-beating is induced when using the knobs. Figure 8b shows that for the maximum dephasing of $25\,^\circ$ a relative β-beating of less than $2\,\%$ is induced in IP7.

Using the maximum de-phasing applied in B1, the variation of the strength of the trim quadrupoles have been calculated. The maximum variation of 1.83×10^{-3} in k_{QT} was identified. This exceeds the preset software tolerance of 1.2×10^{-3}. Therefore, for the purpose of the MD, the restrictions on the powering of the trim quadrupoles have been loosened to accommodate the needed dynamic range.

Finally, tracking simulations in Fig. 9 show a slight improvement of the DA when the phase advance of B1 is modified towards the positive quadrant in the $(\Delta\mu_x, \Delta\mu_y)$ space. While the effect is small it agrees with the expectation that, by making symmetric the phase advance of the two beams, the lifetime of B1 is improved.

2.3 Compensation with DC Wires

The solid wire beam-beam compensator have been installed for B2 in both IR1 and IR5. The wires are embedded in collimators that are used during nominal production fills which follow a very strict collimation hierarchy. In details, at IR1 the wires are vertical and embedded in TCTPV.4R1 (top wire) and TCLVW.A5L1 (bottom wire), while at IP5 the wires are
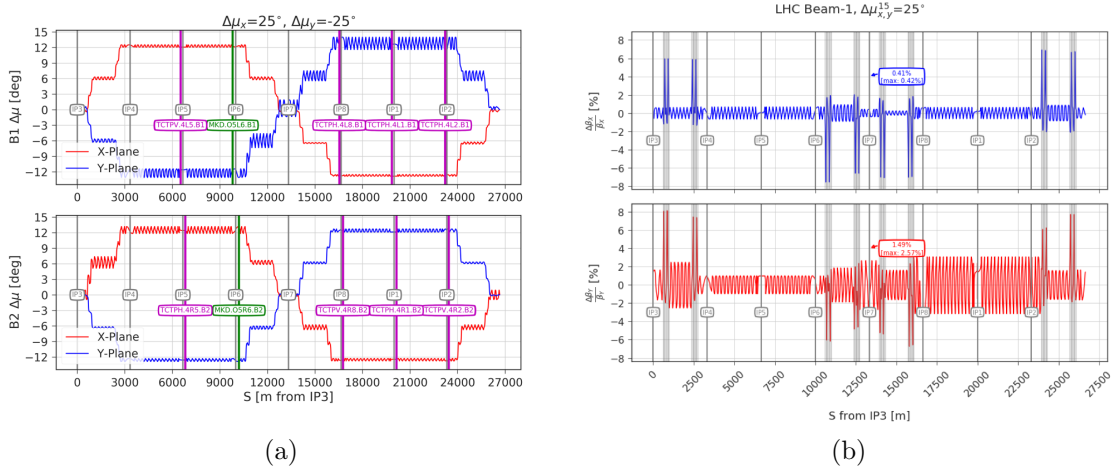
Figure 8: The effect of the de-phasing knob on the phase advance along the ring (a) and on the β-beating that it generates.
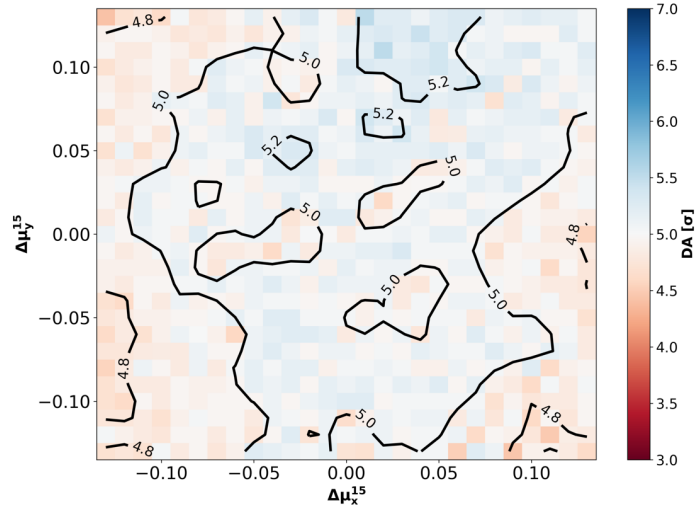

Figure 9: Dynamic aperture simulations for B1 in terms of the variation of the phase advance between IP1/5. A small beneficial effect is found compared to the nominal configuration when $(\Delta\mu_x, \Delta\mu_y)$ are increased with the same sign.

horizontal and are placed at TCL.4L5 (internal) and TCTPH.4R5 (internal) collimators. These collimators are moving when the crossing angle is changed (to follow the beam closed orbit). In this MD, the test of the wire compensator took place at a half-crossing angle of 130 μrad and at β^* of 0.3 m. In this configuration, the position of the left wire in IR5 is at 16.3 σ_{coll} while the right wire at 8.45 σ_{coll}. Targeting a compensation of the octupolar term of the LR beam-beam effects, under this sub-optimal configuration for the wire compensator, the full current (i.e., 350 A) has to be used for all 4 wires as shown in Fig. 10. In this

9

powering configuration of the wires, a compensation of the $\approx 25\,\%$ of the resonance driving term (4,0) is estimated (an ideal compensation would be of 100%).
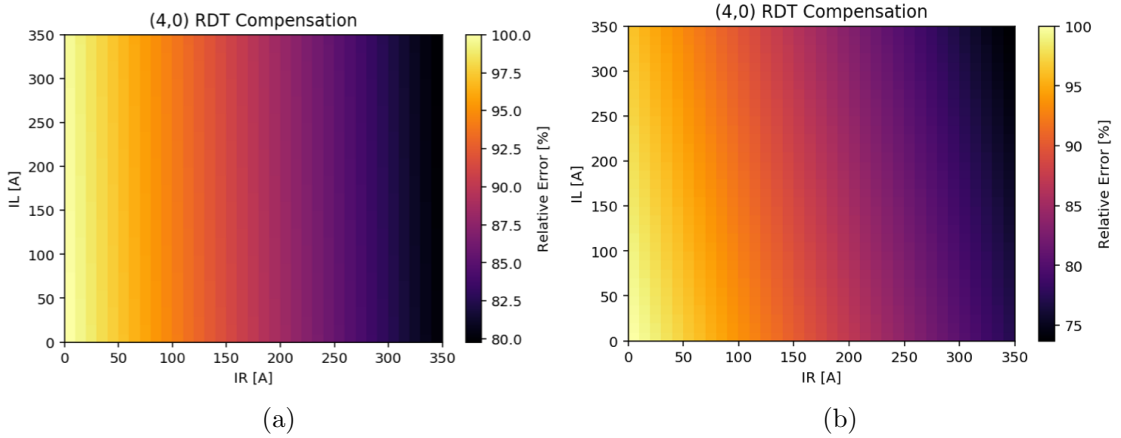

Figure 10: Resonance driving term compensation for the (4,0) term as a function of the wire current for the left, IL, and right wires, IR, of IR1 (a) and IR5 (b). The relative error is color coded and the full compensation corresponds to a relative error of 0 %.

In addition, the already implemented feed-forward system that uses the quadrupoles Q4 and Q5 to perform a local correction of the tune shift induced by the wire, as described in [11] has been used during the MD. In order to slightly improve the configuration for the wire compensator, the movement of the 5$^{\text{th}}$ axis of the wire collimators have been requested. Loss maps taken showed that this movement remains well within the safety margin for machine protection, and was therefore approved.

3 Measurements

The MD took place in the afternoon/night of the 26$^{\text{th}}$ of July, 2018 and spanned over two fills, FILL 6982 and 6984, as shown in Fig. 11. The first fill was used for the measurements of noise at injection energy, while the second focused on the beam-beam effects in collisions. An issue, with the main power supply of the PS, delayed the start of the second fill by almost an hour. However the quick response of the experts allowed the continuation of the MD.

The beam and machine parameters requested for the MD are summarized in Table 1. For FILL 6982 a filling scheme with 133 bunches has been created in order for the total bunch intensity to be sufficient for the needed resolution of the BBQ. On the other hand, for FILL 6984, the beam and machine conditions were requested to be as close as possible to the operational ones during the collision process. The filling schemes for the two fills are shown in Fig. 12.

3.1 FILL 6982

Initially a PILOT bunch was injected in the machine and the EPC expert tested the remote de-activation of the active filters in the main bends. The main observable for this fill is the
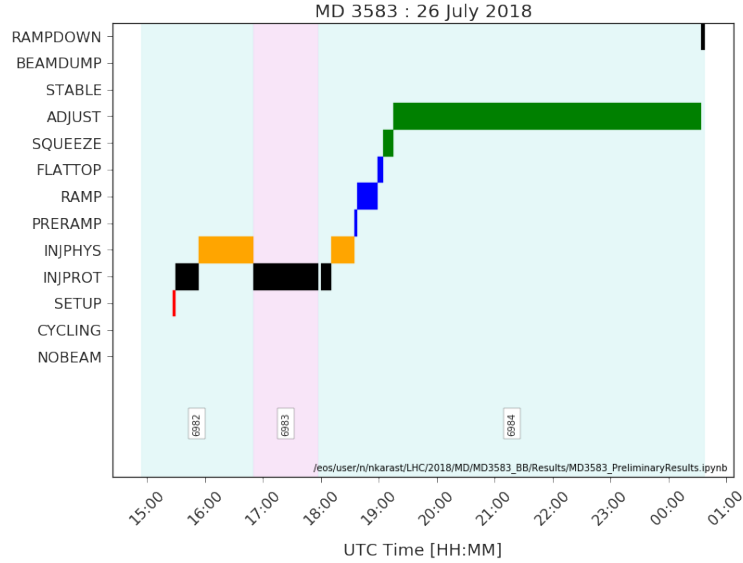
Figure 11: The timeline of the MD 3583 in terms of beam processes. Fill 6982 was used for the test at injection of the active filters, while Fill 6984 was ramped up to top energy for the beam-beam long-range tests.
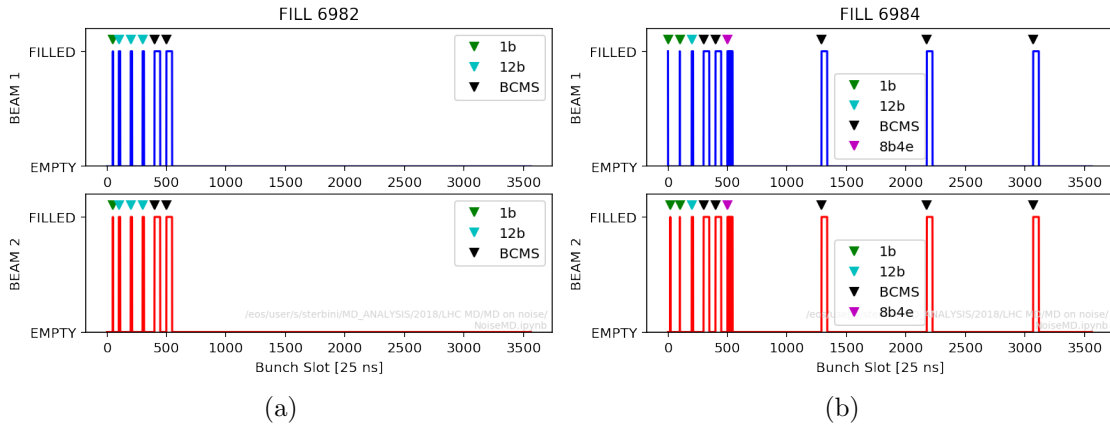

Figure 12: Filling Schemes for Fill 6982 (a) and Fill 6984 (b), for the test of the active filters and the study of the long-range beam-beam effects, respectively.

BBQ spectrum for both beams and both planes. Due to the low intensity of the PILOT bunch and the limited buffer/number of turns of the ADTObsBox, no change on the beam spectrum could be appreciated. This results was expected, but the validation with the PILOT beam was necessary.

After the PILOT bunch was dumped, a train of 12 bunches was injected in the machine and the test with the active filters was repeated. At this stage, no useful signal is observed in the BBQ. However, the second injection proved that the remote activation and de-activation of the active filters of the main dipoles power supplies is safe for the LHC machine protection and therefore the procedure was validated.

Being confident in the procedure after the first tests, the filling scheme prepared for this

11

Parameter	FILL 6982	FILL 6984
Beams Required	1 & 2	1 & 2
Beam Energy [GeV]	450	6500
Optics	Injection	Collisions
Bunch Intensity	1.1×10^{11} ppb	1.1×10^{11} ppb
Number of Bunches	133	285
Transverse Emittance [µm]	1.5	2.3
4σ Bunch Length [ns]	1.0	1.0
Optics Changes	No	No
Orbit Changes	No	Yes (reduced crossing angle)
Collimation Changes	No	Yes (5th axis of wire collimator)
RF system Changes	No	No
Feedback Changes	No	No
Tune Changes	No	Yes
Other Changes	Active Filters	Crossing Bias, B1 Phase Knob, Wire Current, Relax Q4, Q5 limits

Table 1: Beam and machine parameters requested for MD 3583, for both FILL 6982 and 6984.

part of the MD, `25ns_133b_133b_85_0_0_48bpi_FILTER_MD#2`, was injected in order to start the measurements. In each of the 8 sectors the active filters have been switched off and on and the effect on the beam spectrum was observed. Figure 13 shows, for each sector, the powering on (value of 1) and off (value of 0) of the active filters.

The test of the active filters lasted from 15:50 until 16:50 (UTC). Finally, the beams were dumped, the active filters returned at their nominal state and the preparation for injecting the next fill started.

3.2   FILL 6984

This fill was dedicated for the measurements of the BBLR effects. After injecting the prepared filling scheme, `25ns_286b_285_180_180_48bpi_MD3583`, the two beams are accelerated to top energy and brought into collision at a half-crossing angle of 160 µrad and a β^* in IP1 and IP5 of 0.3 m, as in the nominal operation, at 19:15 (UTC). The two beams collide in all 4 IPs, with the variety in terms of bunch types (LHCINDIV, BCMS and 8b+4e trains) having, therefore, a different number of LRs. The encounter schedule for the collisions and the number of LR beam-beam interactions is shown in Fig. 14.

To start the dedicated LR tests, the crossing angle at the IP1/5 had to be reduced to 130 µrad in order to enhance the LR signature. The reduction has been performed in steps of 5 µrad using the operational orchestration. At the end of the crossing angle reduction a luminosity optimization was performed in all IPs to optimize the luminosity signals and guarantee head-on collisions in IP1/5. In addition, a small tune scan was employed in order to optimize as much as possible the beam lifetimes.

The first measurement studied the crossing angle bias started at 20:30. Starting from the
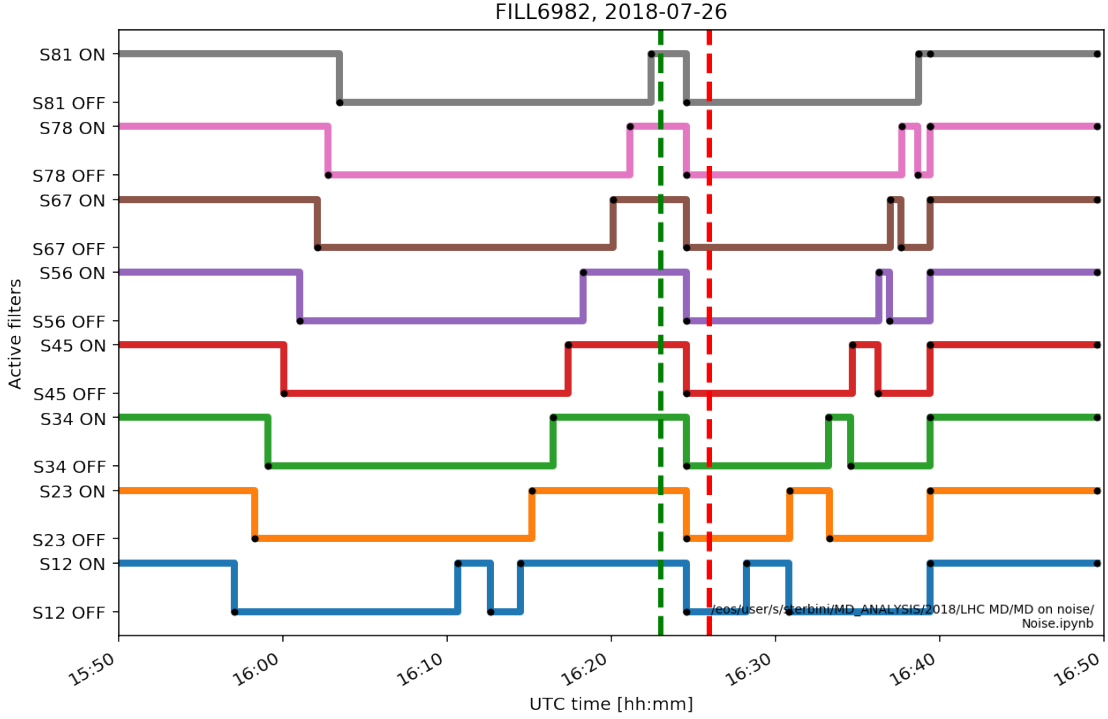
Figure 13: Timeline of the powering on and off of the active filters in the 8 sectors of the LHC.
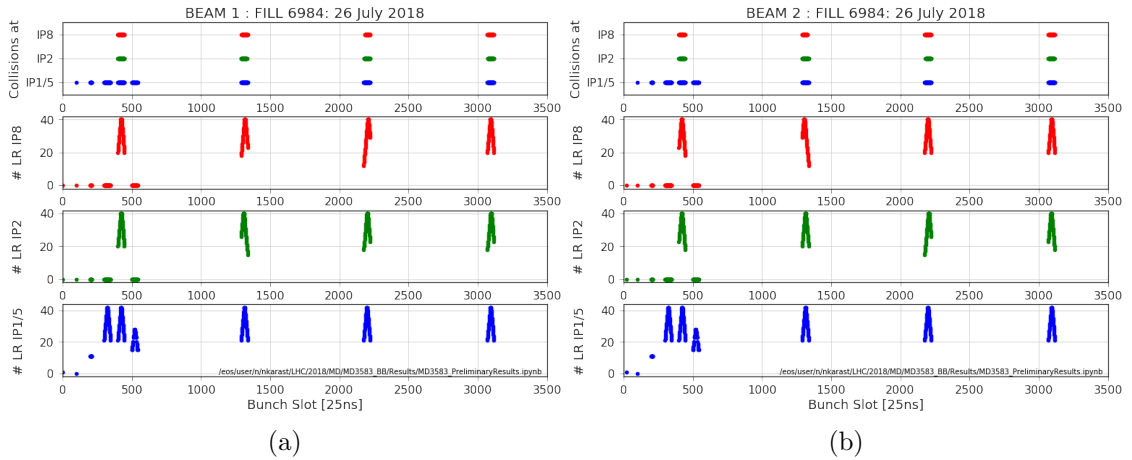

Figure 14: The collision schedule for B1 (a) and B2 (b). The number of long-range beam-beam interactions is plotted versus the bunch slot.

bias in IP5, the knob was tested and the BLM lifetime was observed to identify the impact of the knob. The measurements continued by scanning the crossing bias in IP1.

Due to the initial delay with the power supply of PS, the second and third parts of the MD had been shortened with respect to the than planned time. The scan for the phase advance between IP1 and IP5 started at 22:40 and lasted until midnight. At the start, the phase advance of the vertical plane was varied in small steps around the nominal setting.

13

The horizontal phase advance followed and larger steps in dephasing were introduced. The observable remained the beam lifetime as well as the tune from BBQ. At the end, the trims were reverted and the machine returned to its nominal operation.

The last part of the MD, dedicated to the beam-beam compensation started at midnight and initially required the alignment of the 5$^{\text{th}}$ axis of the wire collimator. Due to the shortage of time, only the right wires at the two IP, which are also the best performing, have been powered to the maximum of their current, i.e., 350 A. Only two cycles of powering on and off have been performed. During the last one the polarity of the lattice octupoles has been reversed.

The test ended with a programmed beam dump at 00.30 and the recovery started to prepare the machine for the next MD. The observations from all the measurements are described in detail in the next section.

4 Results

4.1 FILL 6982

4.1.1 INJPHYS

This test was done in preparation for the MD4147, performed during the fourth MD block of 2018. The active filter, AF, of the converters powering the 8 sectors of the Main Bend (MB) circuits are always switched on in normal operation. During this MD they were sequentially switched off. This allowed to analyze the evolution of the voltage and current signal of the power converters, PC (Fig. 13). As an example, we reported in Fig. 15 the voltage/current evolution of the Sector12 PC. This is a 1 kHz sampled signal obtained directly from the PC control circuit. A clear effect of the AF on the PC voltage is visible, whereas the PC current signal effect is dominated by noise.

After having injected the beam trains and having repeated the switch ON-OFF commutation of the AFs, the signature of the AF was also visible on the beam spectrum. In Figs. 16, 17, 18, 19 the spectra for the two beams in the two planes are shown. The B1 horizontal spectrum is perturbed by some instrumental noise (vertical lines). Nevertheless, for both beams and planes the amplitude variation of the 50 Hz line of the spectra depends on the status of the AF. This was another important and clear evidence that the noise lines harmonics of 50 Hz lines are not an instrumental effects. In addition, it showed that the PC noise is visible in the beam up to relative high frequencies, larger than 1 kHz (mainly multiples of 600 Hz).

4.2 FILL 6984

4.2.1 INJPHYS to ADJUST

The 286 bunches injected in the machine had an average intensity of $(1.03 \pm 0.06) \times 10^{11}$ ppb for B1 and $(1.02 \pm 0.05) \times 10^{11}$ ppb for B2, as shown in Fig. 20a, which makes them very close to the operational bunches at the time. Similar intensities are found among the BCMS and 8b+4e trains.
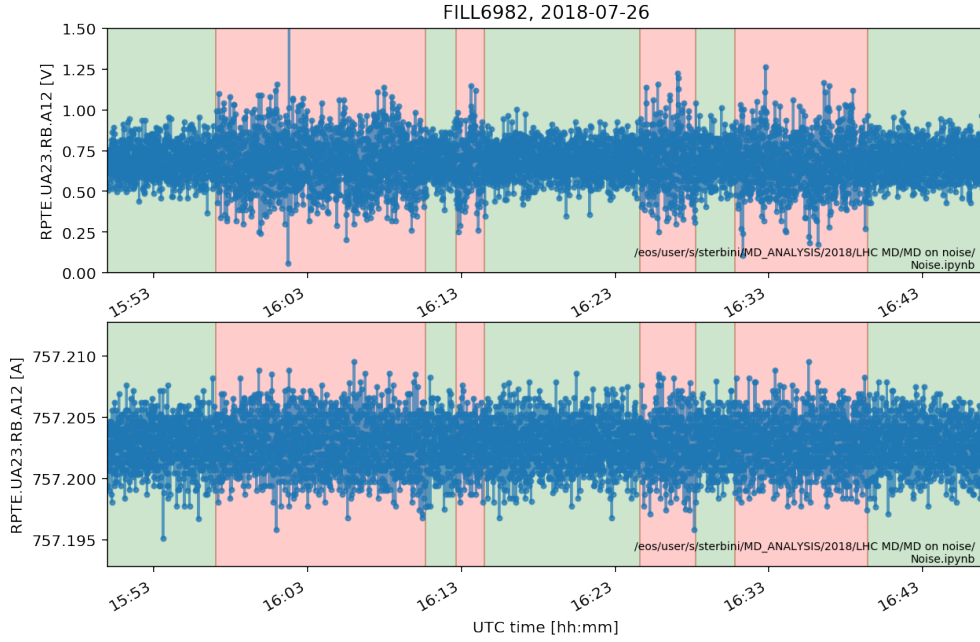
Figure 15: Voltage and current measured on the PC of the Sector12 MB. The green and the red areas represent the time windows when the AF were on and off, respectively.

According to the injection BSRT measurements, both beams were round in the transverse plane, with an average emittance of B1 of (1.41 ± 0.14) µm and of (1.13 ± 0.14) µm for B2. The bunch-by-bunch emittances at the moment of injection are shown in Fig. 21. In both beams the 12b train seems to be injected with higher emittance, which explains the lower brightness shown in Fig. 20b. On the other hand the BCMS trains show similar spread in intensity and emittances, but they do exhibit, within a train, a gradual increase of emittance. This behaviour is usually attributed to the impact of electron cloud. However, the 8b+4e bunches, which should be less affected by the electron cloud, due to the more frequent bunch spacing, exhibit the reverse behaviour. In both beams and both planes, running along the 8b+4e train the emittances seems to be decreasing.

The evolution of the emittances during the Flat Bottom (FB) plateau is shown in Fig. 22a. In both beams and planes the sudden increase of emittance is due to the injection of the 12b train which have significantly larger emittance than the rest of the bunches. The average is then reduced when the first BCMS train is injected. The overall relative blow-up along the injection plateau is shown in Fig. 21b. The blow-up is calculated for each bunch as the relative difference between the first and the last BSRT measurement. The data follow the trend, observed also in production fills, that the horizontal plane blows up more than the vertical and B1 increases more than B2. Apart from the horizontal plane of B1, the 8b+4e bunches seem to blow-up less than the BCMS ones. This is expected since the electron cloud contribution in the emittance blow-up is smaller compared to the BCMS beams due to the increased number of bunch spaces. The bunches of the 3 last BCMS trains have been injected towards the end of the injection plateau and thus the blow-up is less.

In terms of losses, the average loss rate for the two beams from the time of injection until right before the start of collisions is shown in Fig. 23a. The loss rate is defined using
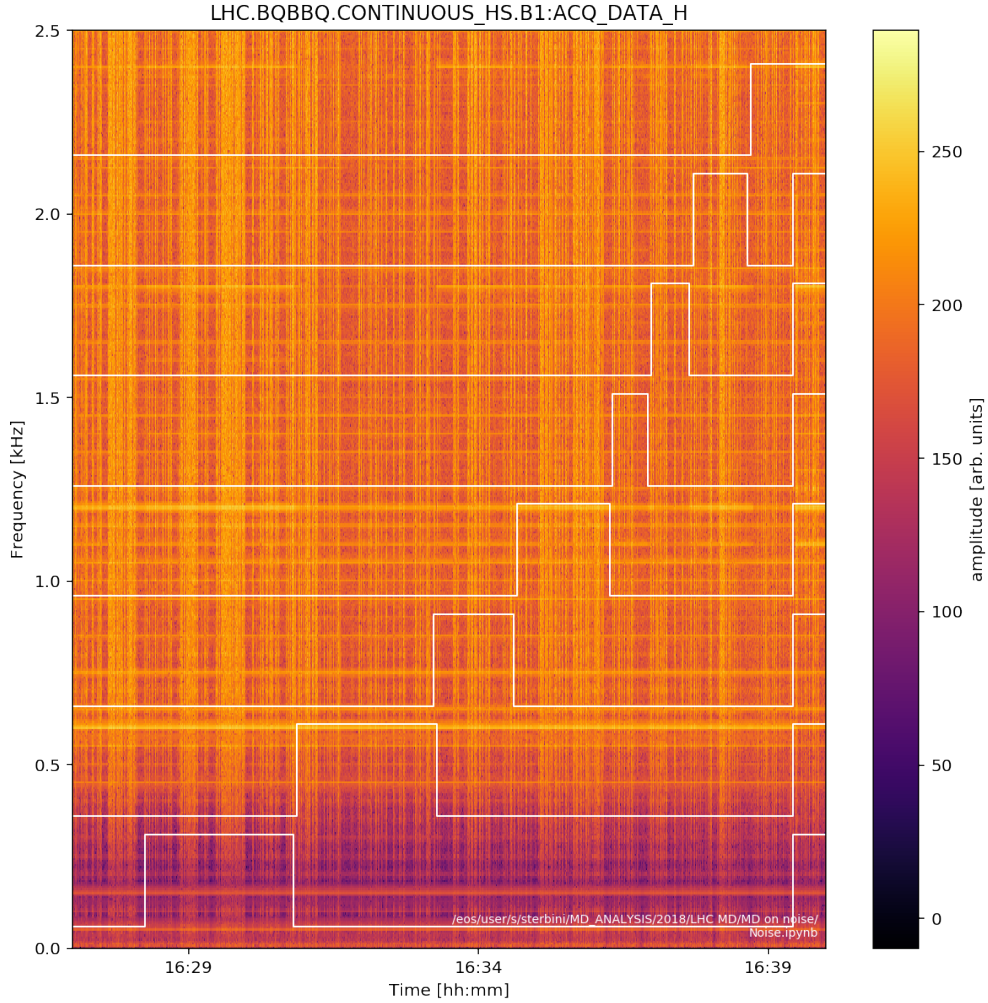
15

Figure 16: B1 horizontal spectrum from the high sensitivity BBQ. The white lines represent the status (as shown, in a larger time window, in Fig. 13) of the active filters corresponding to the power converters of the eight LHC sectors. The harmonics of 600 Hz appear to be more affected than the others harmonics by the active filters settings.

measurements from the FBCT. Since during the INJPHYS process new bunches are continuously injected, the variation in intensity fluctuates significantly. After the injection plateau a significant amount of losses takes place at the end of the RAMP. Using the diamond BLM (DBLM) data the increased losses can be seen for the first two BCMS trains and the 8b+4e train in Fig. 23b. B1 is affected more than B2. The bunch-by-bunch pattern of the losses do not suggest any beam-beam related source of losses. The fact that the end of the trains seem to have a larger amount of losses compared to the head of the trains, suggests that the bunches at the end of the train, which have larger emittances are losing more. Orbit effects that induce slight scraping to B1, could explain the observations. However, the studies have to be complemented with emittance measurement during the RAMP, which is not possible with full beam, as well as the beam losses decomposition in the two planes.
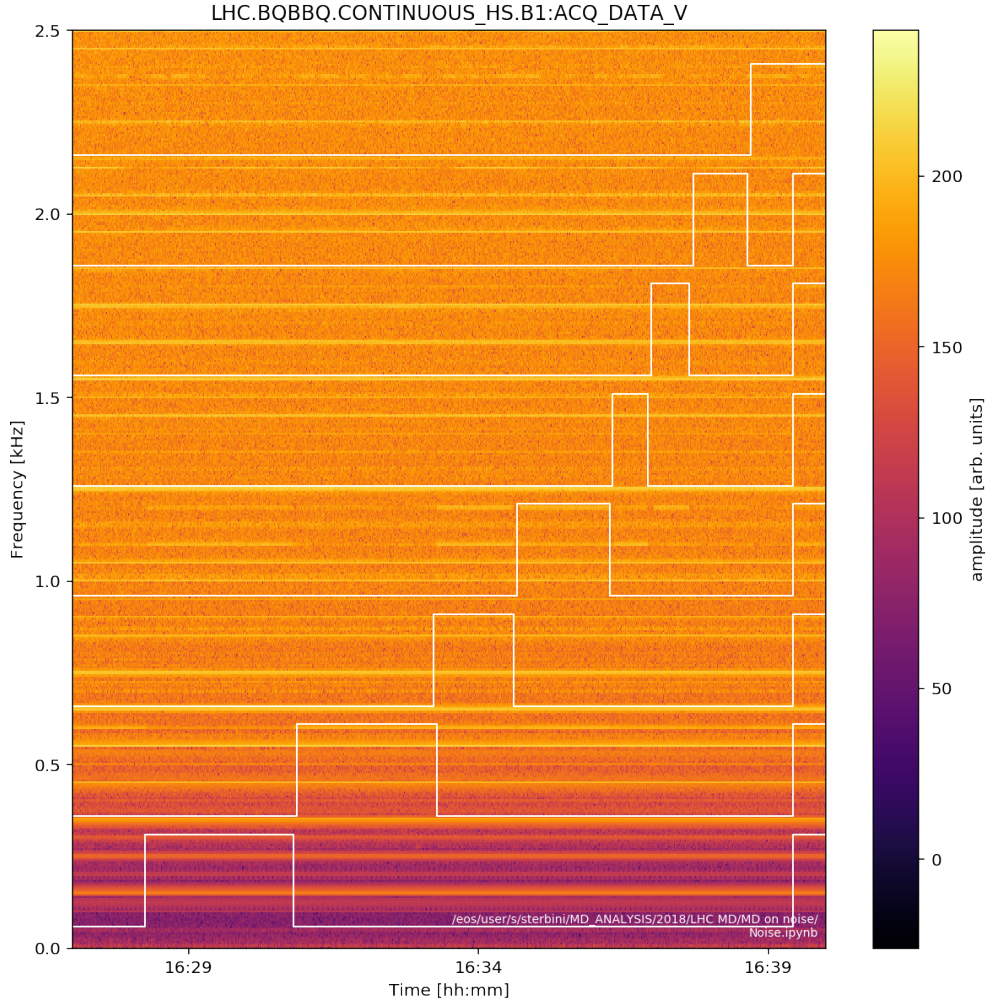
Figure 17: B1 vertical spectrum from the high sensitivity BBQ. The white lines represent the status (as shown, in a larger time window, in Fig. 13) of the active filters corresponding to the power converters of the eight LHC sectors.

4.2.2 ADJUST

4.2.2.1 Overall Observables and Instrumentation Issues

The collisions started in ADJUST beam mode at 160 µrad half-crossing angle in IP1 and IP5 at β^* of 0.3 m. Bunch-by-bunch luminosity signals have been requested from all IPs. The evolution in luminosity of ATLAS and CMS, along the whole duration of the MD is found in Fig. 24. While the ATLAS measurements look reasonable, the CMS luminosity recording was found to be fluctuating significantly which makes the data unusable for offline analysis. In order to have an estimate, ATLAS and CMS are assumed fully symmetric and the signal from ATLAS luminosity is used for both experiments, wherever it is required.

The evolution of the average bunch intensity and beam lifetimes are shown in Fig. 25. A drop of lifetime especially in B1 is observed during the crossing angle reduction, which slightly recovers when the tune is optimized. Only small impact in the lifetime evolution is
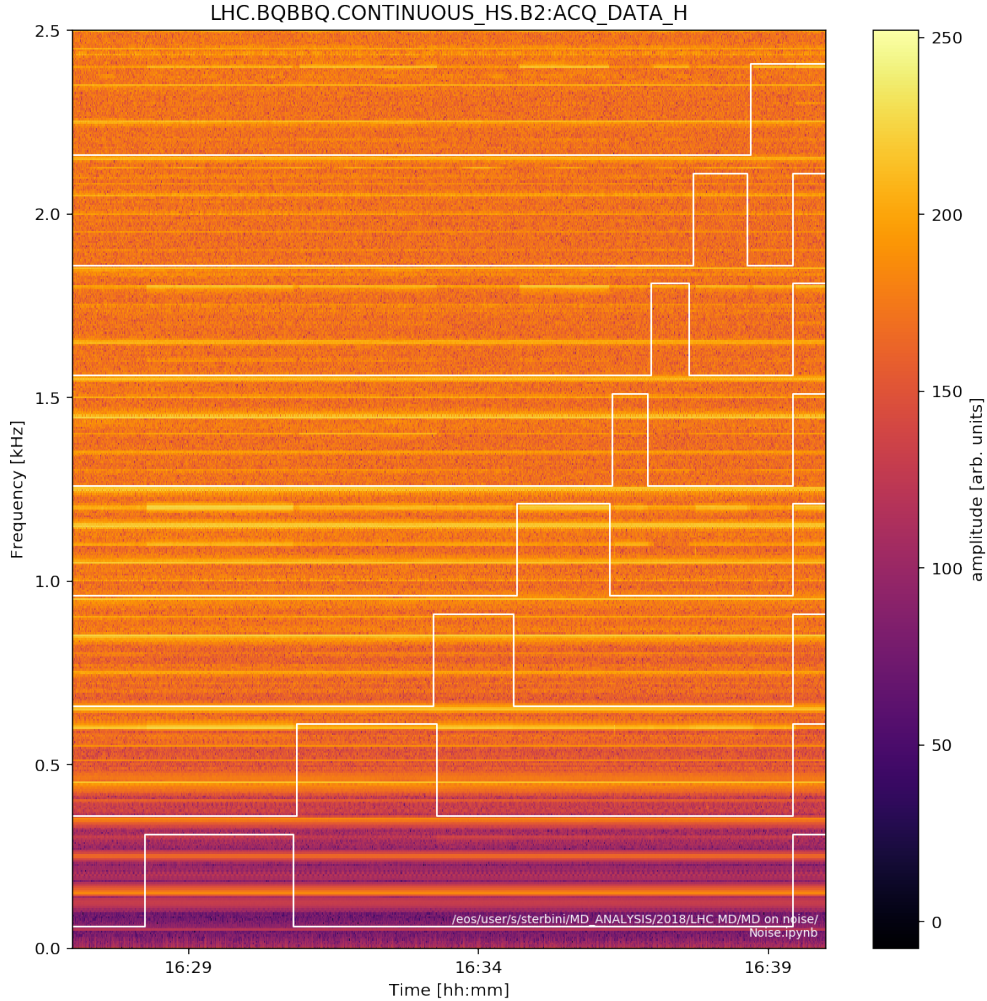
17

Figure 18: B2 horizontal spectrum from the high sensitivity BBQ. The white lines represent the status (as shown, in a larger time window, in Fig. 13) of the active filters corresponding to the power converters of the eight LHC sectors.

found along the various tests. The exceptions are the reduction in lifetime at the end of the phase advance scan for B1, and at the end of the wire compensator test. The ratio of the two lifetimes remained away from unity with B1 suffering more losses than B2 throughout the MD. Finally, the time-periodic spikes on the evolution of the lifetime are found to be attributed to the spikes in the CMS luminosity seen in Fig. 24, since the BLM lifetime calculation takes into account the luminosity signals of the two experiments to compute the burn-off corrected lifetime.

Concerning the evolution of the emittances, Fig. 26 shows the measurements for both beams and planes. The measurement for B2 seems inconsistent with the measurements at the start of the RAMP. Table 2 shows the statistics on the measured emittance values at the end of the Flat Bottom plateau and at the start of collisions. While B1 shows a blow-up of 34 % in the horizontal and 4 % for the vertical plane, B2 shows a damping of 16 % in the horizontal and no blow-up in the vertical plane. The measurement suggest a possible issue
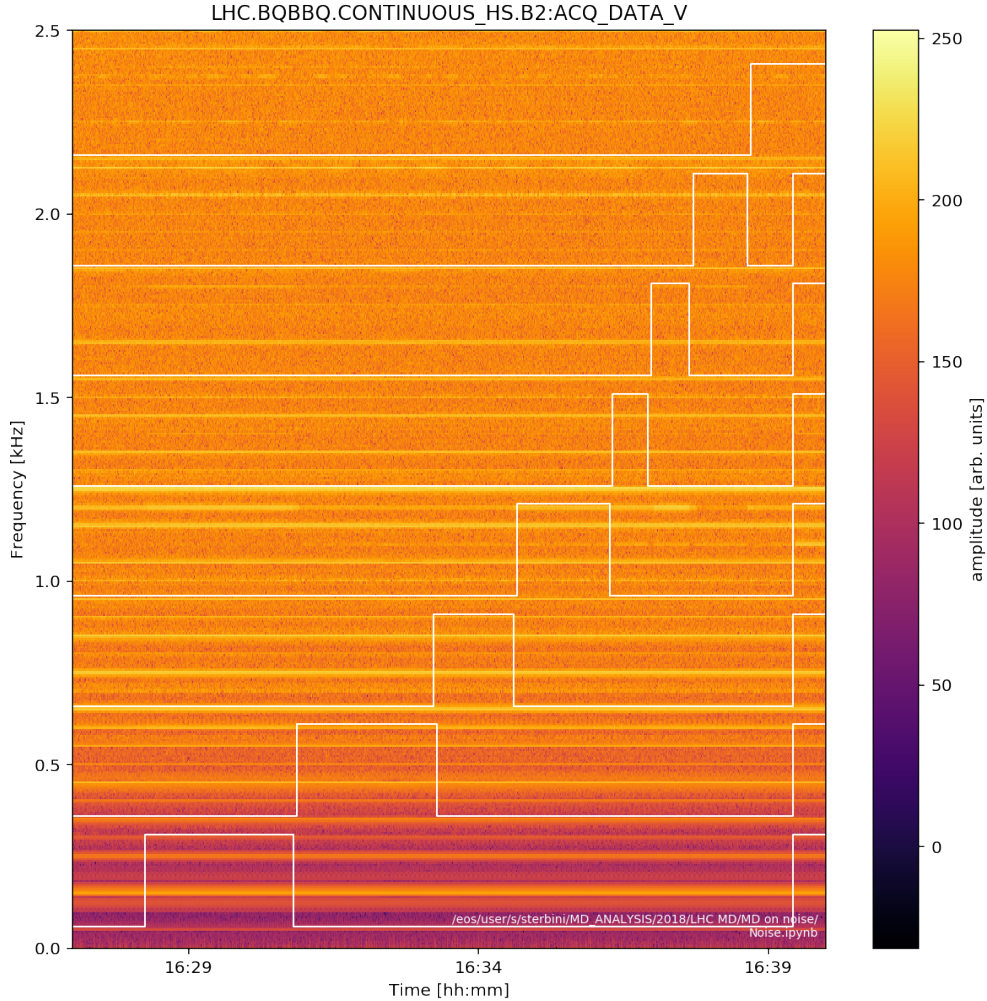
Figure 19: B2 vertical spectrum from the high sensitivity BBQ. The white lines represent the status (as shown, in a larger time window, in Fig. 13) of the active filters corresponding to the power converters of the eight LHC sectors.

with the calibration of the BSRT instrument. Therefore the measurement of the emittance evolution can only be used for relative comparison between bunches.

4.2.2.2 Reduction of the Crossing Angle

In order to enhance the effect of the beam-beam interactions, the half-crossing angle in the two high-luminosity IPs was first reduced from $160\,\mu\text{rad}$ to $130\,\mu\text{rad}$ in steps of $5\,\mu\text{rad}$. Figure 27a shows the DBLM loss rate for the first three trains of the two beams. The reduction of the crossing angle shows a clear LR signature in B1, with the center of the BCMS trains, which demonstrate the most LR interactions, suffering more than the tails of the trains. On the other hand, B2 seems more resilient in the LR beam-beam effects. On the same direction, the 8b+4e train show significantly less losses compared to the BCMS ones. Taking the cumulative integral along the time axis, Fig. 27b reveals that the impact of the LR interactions in B1 are 2.9 times more pronounced. In addition, the second BCMS train
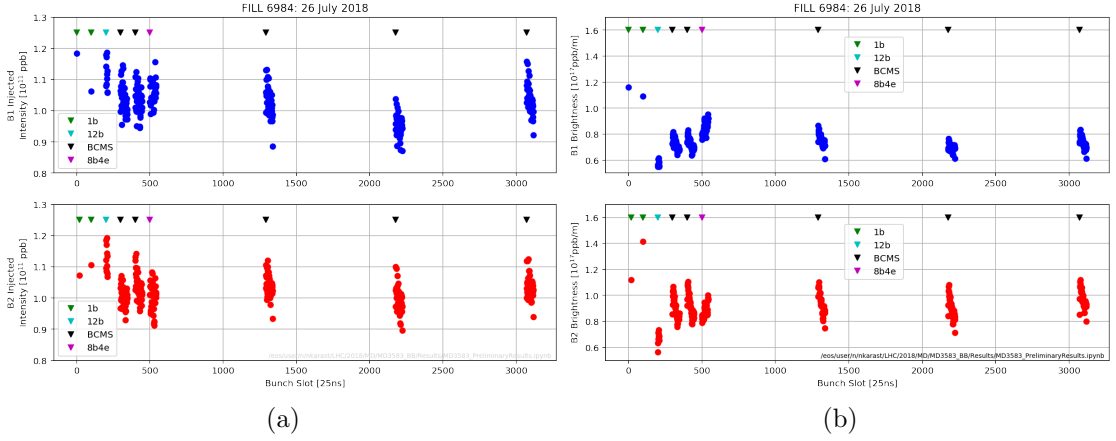
19

Figure 20: The injected intensity (a) and injected brightness (b) for the bunches of the two beams.
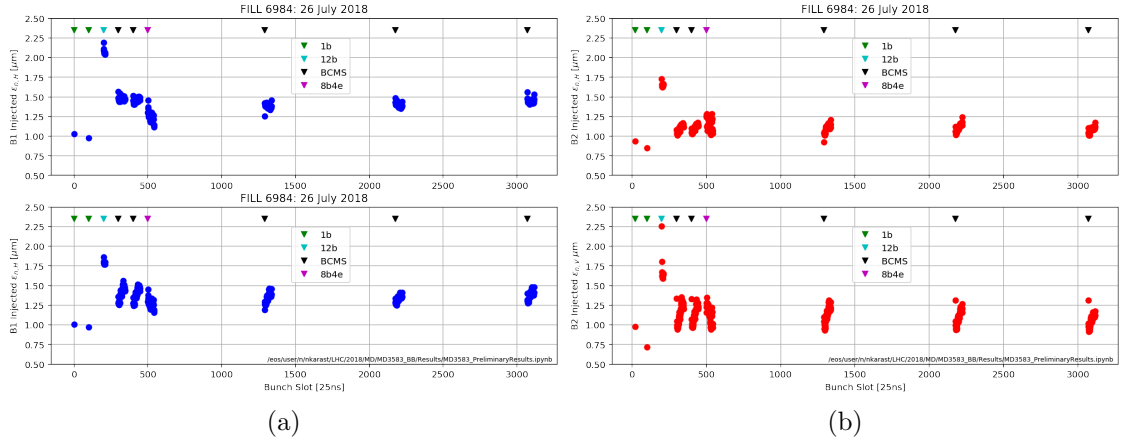

Figure 21: The injected emittances for B1 (a) and B2 (b).

collides not only in IP1 and IP5 but also in the other two IPs. The impact of the other two IPs in terms of losses, are negligible. Similar results can also be observed using the FBCT.

4.2.2.3   Crossing Angle Bias Scan

After a mini tune scan, the crossing angle bias scan started from IP5, scanning both positive and negative bias values before moving on to IP1 and combinations of the two IPs. Figure 28a shows the bias trims together with the evolution of the BLM lifetime for the two beams. Looking at the ratio of the lifetimes of the two beams, a modest improvement (most likely due to the loss halo particles in the previous measurement step) is found when the bias knob at IP1 is set to $-17\,\mu$rad and the IP5 knob to $12\,\mu$rad. Alternating between $17\,\mu$rad and $-17\,\mu$rad in IP1 a drop of beam 1 lifetime is found for the positive polarity, while an increase for the negative polarity of the bias knob. B2 lifetime is not affected during this interval. In all cases the ratio of the two beam lifetimes remains constantly below 0.95 during the full
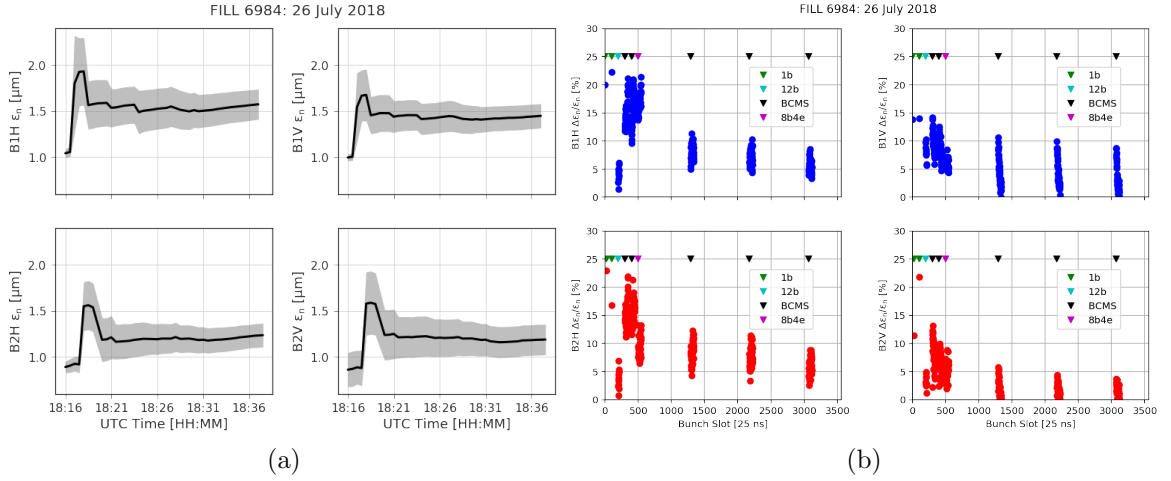
Figure 22: (a) Evolution of the emittances during the injection plateau. The bump at the evolution arises from the injection of the 12b train. (b) The percent blow-up of the emittances during the injection plateau.
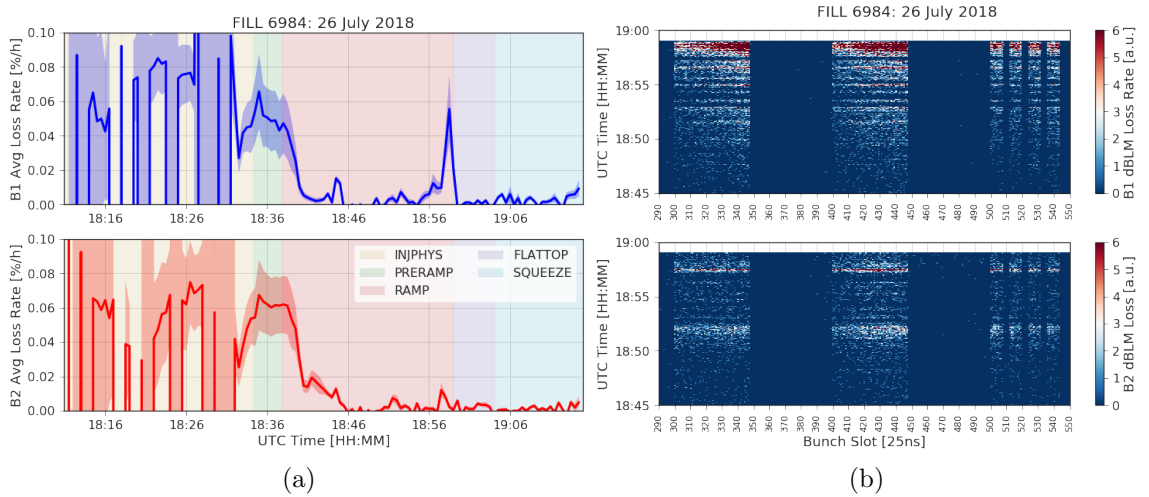

Figure 23: Integral loss rate evolution during the fill (a) and bunch-by-bunch DBLM signal in the second part of the ramp.

scan.

The DBLM data in Fig. 29 show the impact of the knob for the first three bunch trains. While the trains of B2 seem not affected at all, when the bias knob in IP1 was set to 17 µrad, i.e., the B1 (2) crossing angle is at 147 µrad (113 µrad), B1 started demonstrating increased LR beam-beam effects. Reversing the polarity of the knob suppresses these effects. It is not fully clear if the small increase in lifetime is an effect of the knob setting or the reversal of a trim that diminished the lifetime. The effect of the IP5 knob is not affecting the results significantly.

To identify the orbit variation when using the crossing angle bias knob, the DOROS BPM has been used and shown in Fig. 30. The orbit shift remained small (e.g., a variation of
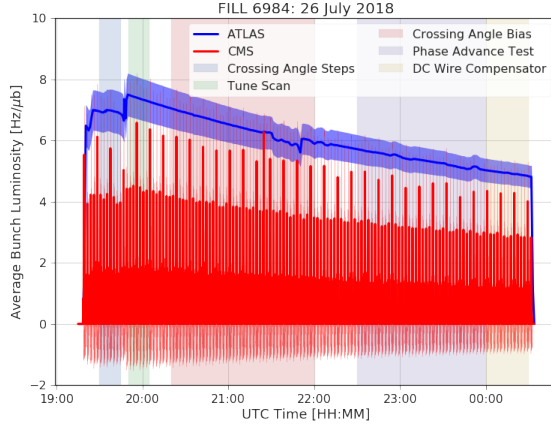
Figure 24: Evolution of the average bunch luminosity recorded by ATLAS and CMS during FILL 6984.
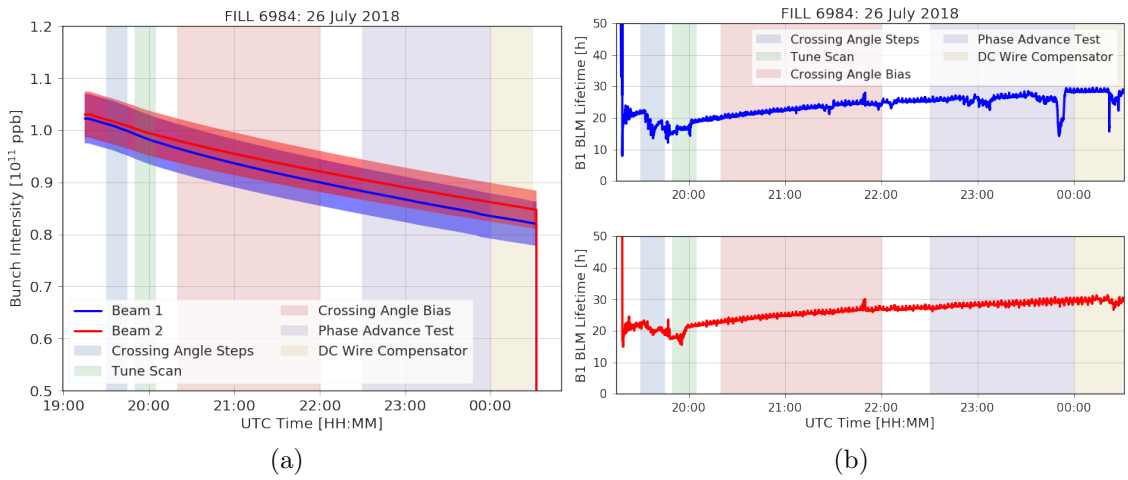

Figure 25: Evolution of the average bunch intensity (a) and BLM lifetime (b) during FILL 6984.

$\approx 0.4\,\sigma_{\mathrm{coll}}$ is produced during the luminosity optimization scans). Focusing at the IP1 DOROS when the knob alternates between $\pm 17\,\mu\mathrm{rad}$ a small orbit jitter is observed. However, the overall result is not clear enough to suggest an operational settings change and further studies are required.

4.2.2.4 IP1 & IP5 Phase Advance

The bias scan started by simultaneously varying the horizontal and vertical phase advance of B1, before testing other settings. No setting that improves the lifetime imbalance was found, as shown in Fig. 31a. However, the bunch-by-bunch measurements in Fig. 31b show that increasing the phase advance in the positive quadrant of the $(\Delta\mu_x,\,\Delta\mu_y)$ space (in the time window $\approx$23:00-23:07) increase the B1 losses along all the bunches of the train. In fact, the effect does not seem to be LR correlated since all the bunches of the train lose
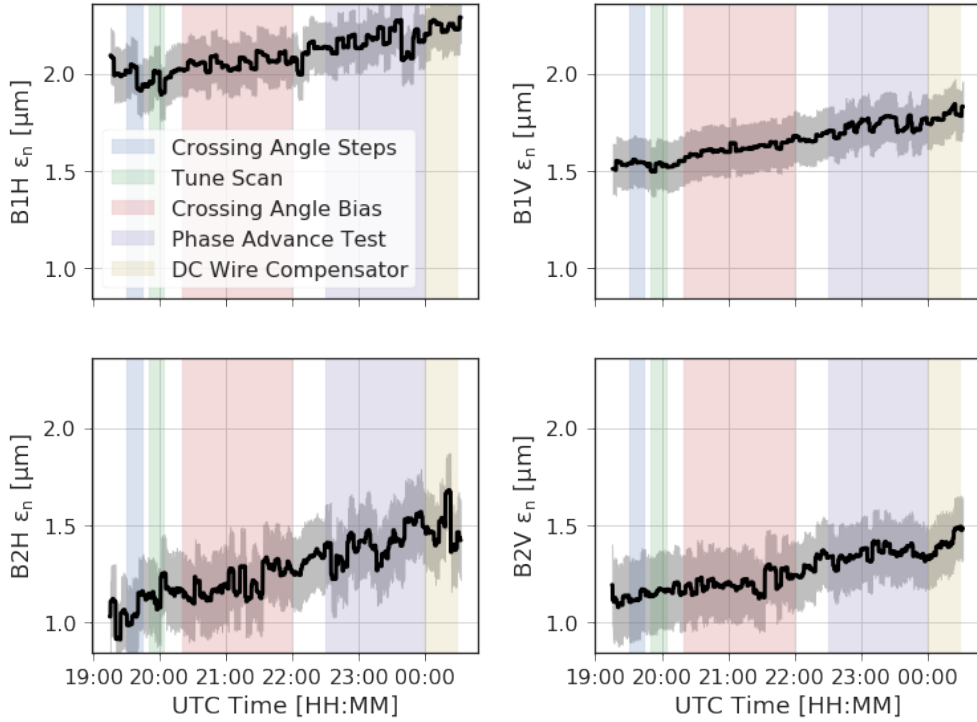
Figure 26: Evolution of the average bunch emittances for the two beams and the two planes for FILL 6984.

the same and also similar losses are found in both the BCMS and 8b+4e trains. The tune measurements are also shown with the data of the continuous high-sensitivity BBQ after a rolling mean sampling. When the knob is at the maximum setting of $\pm 25\,^{\circ}$ (in the time window $\approx$23:30-23:50) a significant offset in the tune, correlated with the phase advance knob, is observed.

4.2.2.5 Beam-Beam Compensation

After the 5-th axis alignment of the wire collimators, the wire demonstrators were powered using the full beam. With a sub-optimal configuration, the full current (350 A) was used to provide some visible results. No significant impact was found in the global lifetime, however

Beam-Plane	Start of RAMP	Start of Collisions
B1 $\varepsilon_{n,H}$ [μm]	1.57 ± 0.16	2.10 ± 0.14
B1 $\varepsilon_{n,V}$ [μm]	1.45 ± 0.13	1.51 ± 0.13
B2 $\varepsilon_{n,H}$ [μm]	1.23 ± 0.13	1.03 ± 0.18
B2 $\varepsilon_{n,V}$ [μm]	1.19 ± 0.16	1.19 ± 0.21

Table 2: The normalized emittances for both beams and planes at the start of RAMP and at the start of Collisions.
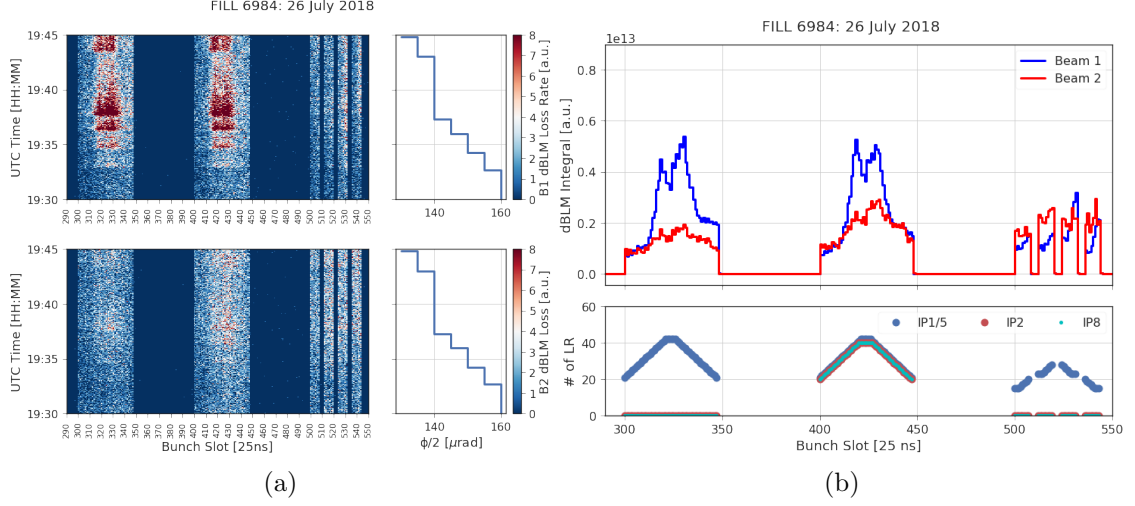
Figure 27: Evolution of the losses for the first two BCMS trains and the 8b+4e train for FILL 6984 (a). The cumulative integral of the DBLM loss rate for the first three trains during the crossing angle reduction (b).
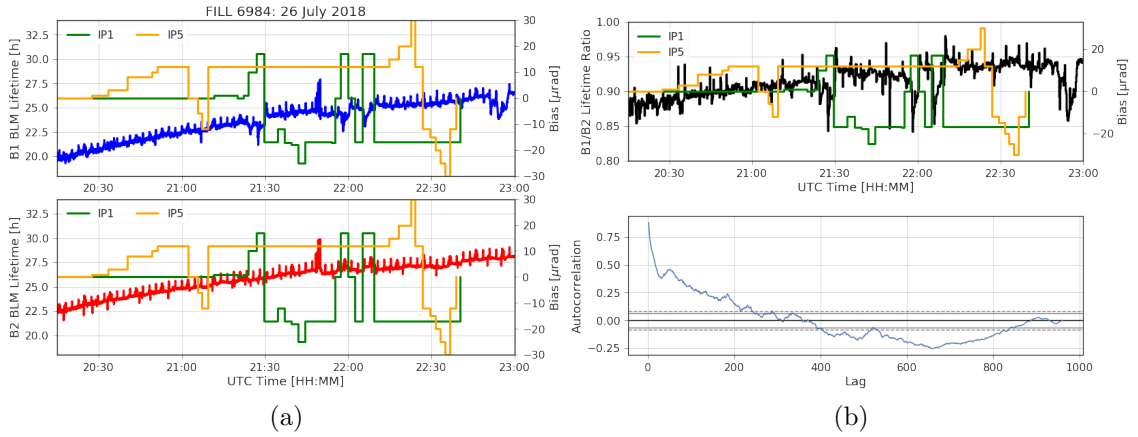

Figure 28: (a) The impact of the IP1 and IP5 crossing angle bias at the evolution of the lifetime as measured by the BLM system. The ratio of the lifetime of B1 over B2 is shown in (b) with the autocorrelation plot of the time series. The solid and dashed gray lines represent the 95 % and 99 % confidence intervals.

the bunch-by-bunch result in Fig. 32 show a clear correlation of the reduction of LR related losses with the powering of the right wires at IP1 and IP5. The reduction of the octupoles and, especially, during the reversal of the polarity around 0 A results in a drop of lifetime. The effect is visible both for beam 1 and beam 2.

5   Conclusions

Despite the initial hiccup with the injectors, the MD3583 ran smoothly. With the first fill, the active filter test showed their clear impact on the beam spectrum. The experience gained
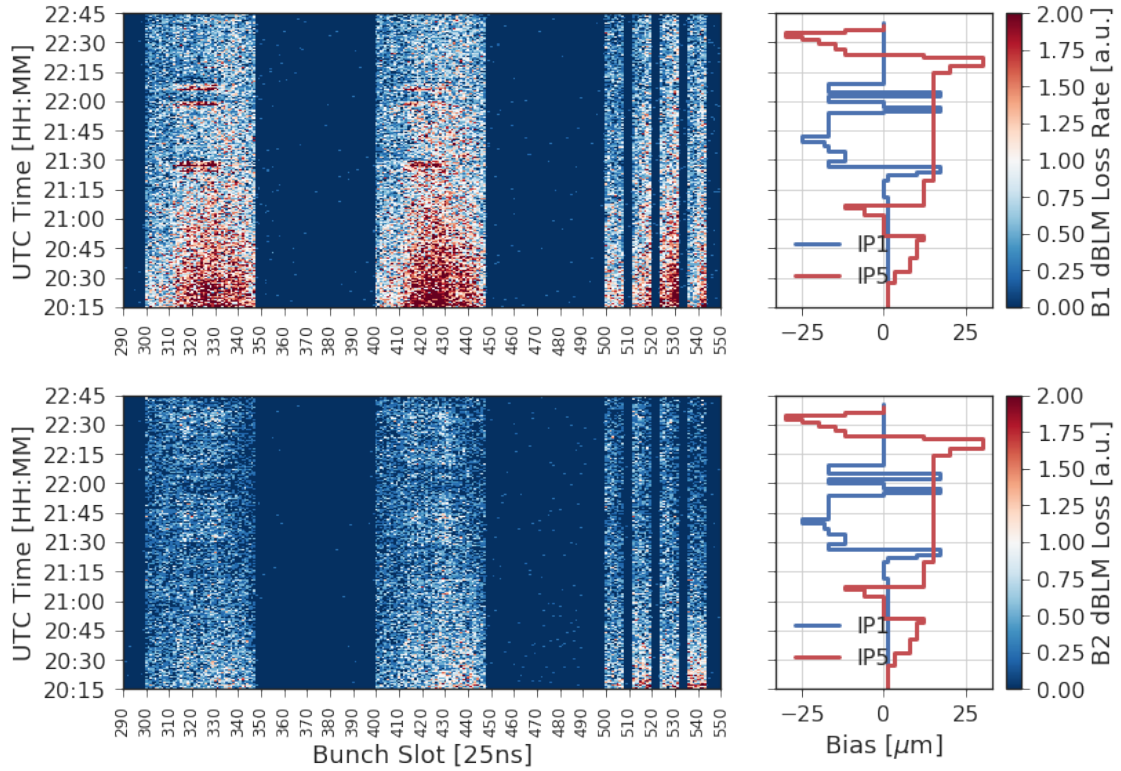
Figure 29: The DBLM loss rate for both beams, focusing on the first three trains.

during this test was important for the preparation of MD4147. The reduction of the crossing angle confirmed the larger sensitivity of B1 to the beam-beam effect (for the BCMS trains but not for the 8b4e one). Concerning the investigation of this B1/B2 asymmetry, despite the different measurement performed (crossing angle bias and IP1/IP5 phase advance scan), the source of the asymmetry could not be clearly identified. A positive IP1 crossing bias and positive IP1/5 phase advance trims appear to have negative effect on the B1 lifetime (increasing even more the asymmetry of the two beams). In the last part of the MD, for the first time, the wire demonstrator were tested with trains. The DBLMs signals showed that a modest reduction of beam losses can be achieved, opening the way to further studies and measurements.
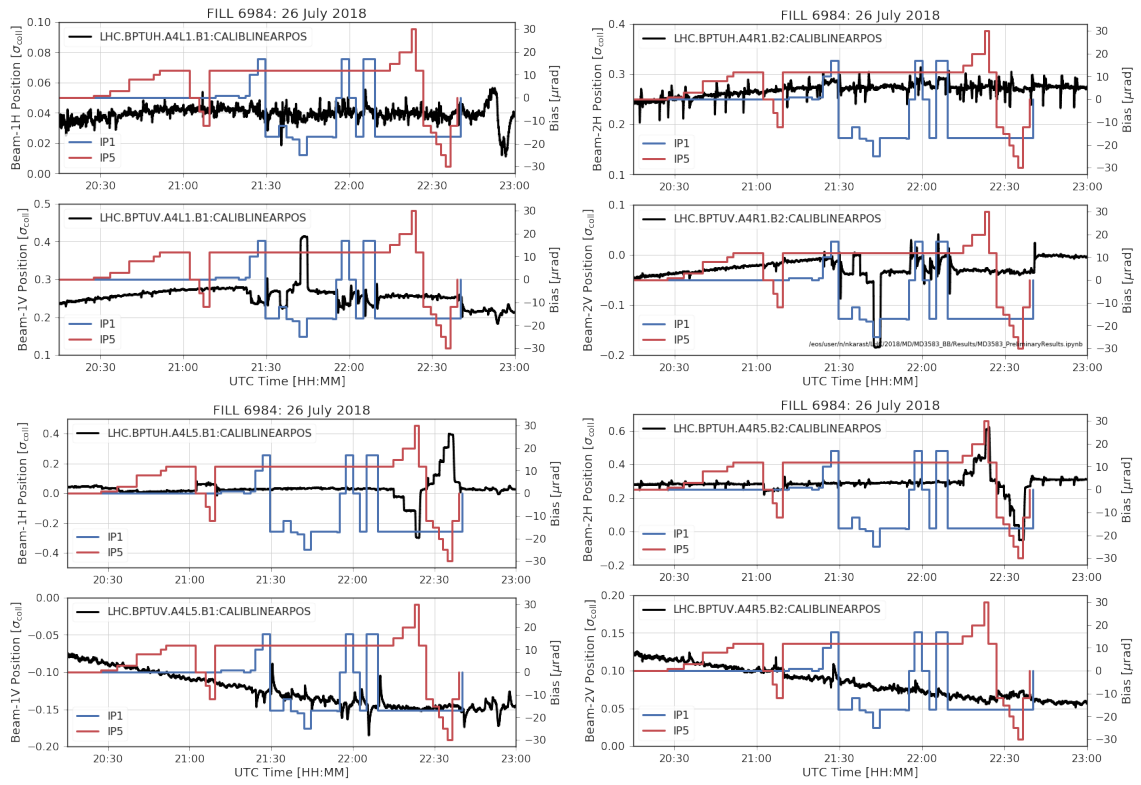
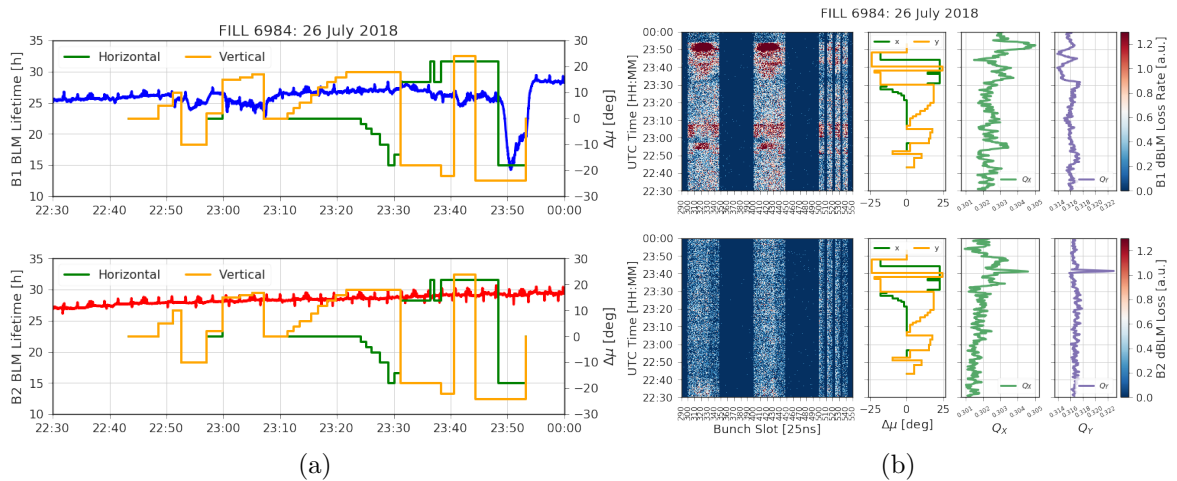Figure 30: The beam position using the DOROS BPM at IP1 (top) and IP5 (bottom) for the two beams.

Figure 31: The effect of the phase advance knob in the total BLM lifetime (b) and in the bunch-by-bunch measurements (b). The effect of the knob on the tune setting is shown.
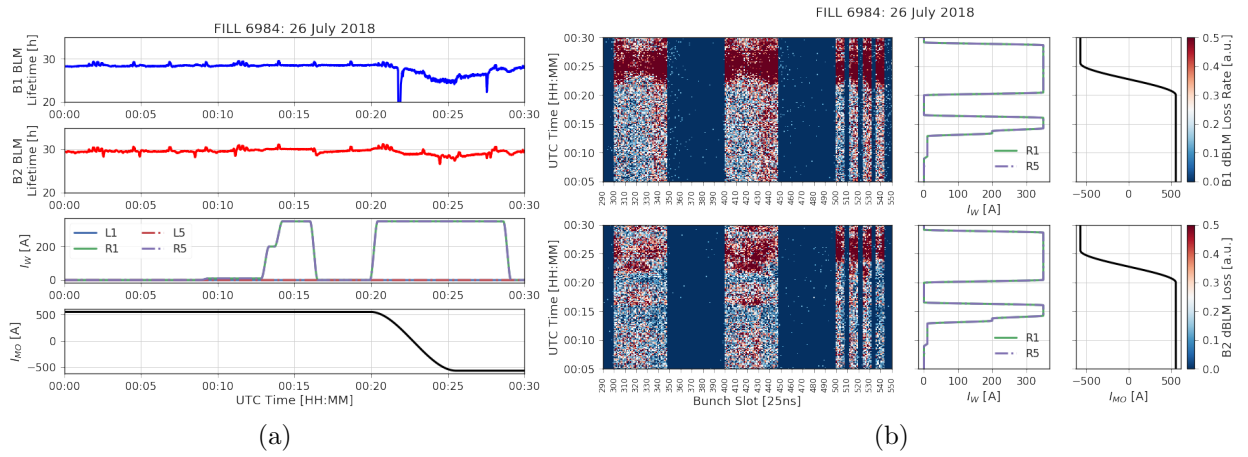
26

Figure 32: The effect on the lifetime of the wire compensation (also combination with the octupole scan) is shown (a) together with bunch-by-bunch losses from the DBLM (b). From the B2 DBLM signal is possible to observe a partial compensation of the wires (in the time window ≈00:12-00:17).

6 Acknowledgements

References

[1] W. Herr, E. Maclean, E. Metral, N. Mounet, G. Papotti, R. Tomas Garcia, and J. Wenninger. Chromaticity dependence on octupole strength. Sep 2012.

[2] W. Herr, X. Buffat, R. Calaga, R. Giachino, G. Papotti, T. Pieloni, and D. Kaltchev. Long Range Beam-beam Effects in the LHC. In *Proceedings, ICFA Mini-Workshop on Beam-Beam Effects in Hadron Colliders (BB2013): CERN, Geneva, Switzerland, March 18-22 2013*, pages 87–92, 2014.

[3] T. Pieloni, J. Barranco, X. Buffat, S. M. White, J. Qiang, G. Arduini, E. Metral, N. Mounet, and D. Banfi. Two beam effects. pages 69–80. 12 p, 2014.

[4] T. Pieloni, D. Banfi, J. Barranco, M. Crouch, X. Buffat, C. Tambasco, E. Metral, B. Salvachua, M. Pojer, R. Giachino, M. Solfaroli, and G. Trad. Beam-beam effects long-range and head-on. pages 111–122. 12 p, 2016.

[5] M. Crouch, T. Pieloni, J. Barranco Garcia, D. Banfi, X. Buffat, C. Tambasco, Y. Alexahin, R. Bruce, R. Giachino, M. Pojer, B. M. Salvachua Ferrando, M. Solfaroli Camillocci, and G. Trad. Long range beam-beam interaction and the effect on the beam and luminosity lifetimes. Jan 2016. Research supported by the High luminosity LHC project.

[6] Y. Papaphilippou. LHC Beam quality and its evolution in 2017. In *Chamonix 2018*. CERN, 2018.

[7] Y. Papaphilippou. Long Range Beam Beam effects for the HL-LHC. In *Chamonix 2018*. CERN, 2018.

[8] Giovanni Iadarola, Giovanni Rumolo, Philipp Dijkstal, and Lotta Mether. Analysis of the beam induced heat loads on the LHC arc beam screens during Run 2. Dec 2017.

[9] A. Poyet, S. Fartoukh, N. Fuster Martinez, N. Karastathis, Y. Papaphilippou, M. Pojer, S. Redaelli, A. Rossi, K. Skoufaris, M. Solfaroli Camillocci, and G. Sterbini. MD3263: Beam-Beam Long-Range Compensation using DC Wires in the LHC. 2019.

[10] S. Fartoukh, M. Albert, Y. Le Borgne, C. Bracco, R. Bruce, F. S. Carlier, J. M. Coello De Portugal Martinez Vazquez, A. Garcia-Tabares Valdivieso, K. Fuchsberger, R. Giachino,

E. H. Maclean, L. Malina, A. Mereghetti, D. Mirarchi, D. Nisbet, L. Normann, G. Papotti, T. H. B. Persson, M. Pojer, L. Ponce, S. Redaelli, B. M. Salvachua Ferrando, P. K. Skowronski, M. Solfaroli Camillocci, R. Suykerbuyk, R. Tomas Garcia, D. Valuch, A. Wegscheider, and J. Wenninger. ATS MDs in 2016. 2016.

[11] G. Sterbini, D. Amorim, G. Arduini, H. Bartosik, R. Bruce, X. Buffat, L. R. Carver, G. Cattenoz, E. Effinger, S. Fartoukh, M. Fitterer, N. Fuster Martinez, M. Gasior, M. Gonzalez Berges, A. Gorzawski, G.-H. Hemelsoet, M. Hostettler, G. Iadarola, R. Jones, D. Kaltchev, N. Karastathis, S. Kostoglou, I. Lamas Garcia, T. Levens, A. Levichev, L. E. Medina Medrano, D. Mirarchi, J. Olexa, P. S. Papadopoulou, Y. Papaphilippou, D. Pellegrini, M. Pojer, L. Ponce, A. Poyet, S. Redaelli, A. Rossi, B. M. Salvachua Ferrando, H. Schmickler, F. Schmidt, K. Skoufaris, M. Solfaroli Camillocci, R. Tomas Garcia, G. Trad, A. Valishev, D. Valuch, C. Xu, C. Zamantzas, and P. Zisopoulos. MD2202: compensating long-range beam-beam effect in the LHC using DC wires. 2019.

[12] S. Kostoglou. Analysis and observation of 50 Hz lines in the LHC BBQ system. CERN, 2016.

[13] G. Arduini. 50 Hz lines studies: First Observations. CERN, 2015.